

Research Articles: Systems/Circuits

Increased neural activity in mesostriatal regions after prefrontal transcranial direct current stimulation and L-DOPA administration

Benjamin Meyer^{1,2}, Caroline Mann³, Manuela Götz^{1,2}, Anna Gerlicher^{1,2}, Victor Saase¹, Kenneth S.L. Yuen^{1,2}, Felipe Aedo-Jury^{2,4}, Gabriel Gonzalez-Escamilla⁵, Albrecht Stroh^{2,4} and Raffael Kalisch^{1,2}

¹Neuroimaging Center (NIC), Focus Program Translational Neuroscience (FTN), Johannes Gutenberg University 55131 Mainz, Germany

²Deutsches Resilienz Zentrum (DRZ), Johannes Gutenberg University Medical Center Mainz, 55131 Mainz, Germany

³Department of Child & Adolescent Psychiatry, Psychosomatics and Psychotherapy, University Hospital Frankfurt am Main, Goethe University Frankfurt am Main, 60590 Frankfurt am Main, Germany

⁴Institute for Microscopic Anatomy and Neurobiology, Focus Program Translational Neurosciences (FTN), Johannes Gutenberg University Mainz, 55131 Mainz, Germany

⁵Department of Neurology, Neuroimaging Center (NIC), Focus Program Translational Neuroscience (FTN), University Medical Center of the Johannes Gutenberg-University Mainz, 55131 Mainz, Germany

<https://doi.org/10.1523/JNEUROSCI.3128-18.2019>

Received: 10 December 2018

Revised: 10 April 2019

Accepted: 10 April 2019

Published: 1 May 2019

Author contributions: B.M., A.G., K.Y., F.A.-J., A.S., and R.K. designed research; B.M., C.M., M.G., A.G., K.Y., and F.A.-J. performed research; B.M., V.S., F.A.-J., and G.G.-E. analyzed data; B.M. wrote the first draft of the paper; B.M., C.M., M.G., V.S., A.G., K.Y., F.A.-J., G.G.-E., A.S., and R.K. edited the paper; B.M. wrote the paper; A.S. and R.K. contributed unpublished reagents/analytic tools.

Conflict of Interest: The authors declare no competing financial interests.

This work was supported by the University Medical Center of the Johannes Gutenberg University Mainz and the German Research Foundation DFG (CRC 1193).

Corresponding author: Benjamin Meyer; University Medical Center Mainz; Neuroimaging Center (Geb.701); Langenbeckstrasse 1, 55131 Mainz; email: benmeyer@uni-mainz.de

Cite as: J. Neurosci 2019; 10.1523/JNEUROSCI.3128-18.2019

Alerts: Sign up at www.jneurosci.org/alerts to receive customized email alerts when the fully formatted version of this article is published.

Title

Increased neural activity in mesostriatal regions after prefrontal transcranial direct current stimulation and L-DOPA administration

(Abbreviated title: Neural effects of tDCS and L-DOPA)

Authors / Affiliations

Benjamin Meyer^{1,2}, Caroline Mann³, Manuela Götz^{1,2}, Anna Gerlicher^{1,2}, Victor Saase¹, Kenneth S.L. Yuen^{1,2}, Felipe Aedo-Jury^{2,4}, Gabriel Gonzalez-Escamilla⁵, Albrecht Stroh^{2,4} and Raffael Kalisch^{1,2}

¹Neuroimaging Center (NIC), Focus Program Translational Neuroscience (FTN), Johannes Gutenberg University 55131 Mainz, Germany

²Deutsches Resilienz Zentrum (DRZ), Johannes Gutenberg University Medical Center Mainz, 55131 Mainz, Germany

³Department of Child & Adolescent Psychiatry, Psychosomatics and Psychotherapy, University Hospital Frankfurt am Main, Goethe University Frankfurt am Main, 60590 Frankfurt am Main, Germany

⁴Institute for Microscopic Anatomy and Neurobiology, Focus Program Translational Neurosciences (FTN), Johannes Gutenberg University Mainz, 55131 Mainz, Germany

⁵Department of Neurology, Neuroimaging Center (NIC), Focus Program Translational Neuroscience (FTN), University Medical Center of the Johannes Gutenberg-University Mainz, 55131 Mainz, Germany

Corresponding author: Benjamin Meyer; University Medical Center Mainz; Neuroimaging Center (Geb.701); Langenbeckstrasse 1, 55131 Mainz; email: benmeyer@uni-mainz.de

29 Number of pages: 38

30 Number of figures: 7

31 Number of tables: 3

32 Number of multimedia and 3D models: 0

33 Number of words for Abstract: 246

34 Number of words for Introduction: 649

35 Number of words for Discussion: 1359

36

37 **Acknowledgements**

38 This work was supported by the University Medical Center of the Johannes Gutenberg

39 University Mainz and the German Research Foundation DFG (CRC 1193).

40 **Conflict of interest**

41 The authors declare no competing financial interests.

42

43

44

45

46

47

48

49

50

51

52

53

54

55 **Abstract**

56 Dopamine dysfunction is associated with a wide range of neuropsychiatric disorders
57 commonly treated pharmacologically or invasively. Recent studies provide evidence for a
58 nonpharmacological and noninvasive alternative that allows similar manipulation of the
59 dopaminergic system: transcranial direct current stimulation (tDCS). In rodents, tDCS has
60 been shown to increase neural activity in subcortical parts of the dopaminergic system and
61 recent studies in humans provide evidence that tDCS over prefrontal regions induces striatal
62 dopamine release and affects reward-related behavior. Based on these findings, we used
63 functional magnetic resonance imaging in healthy human participants and measured the
64 fractional amplitude of low frequency fluctuations (fALFF) to assess spontaneous neural
65 activity strength in regions of the mesostriatal dopamine system before and after tDCS over
66 prefrontal regions (n=40, 22 females). In a second study, we examined the effect of a single
67 dose of the dopamine precursor levodopa (L-DOPA) on mesostriatal fALFF values in male
68 humans (n=22) and compared the results between both studies. We found that prefrontal
69 tDCS and L-DOPA both enhance neural activity in core regions of the dopaminergic system
70 and show similar subcortical activation patterns. We furthermore assessed the spatial
71 similarity of whole-brain statistical parametric maps, indicating tDCS- and L-DOPA-induced
72 activation, and more than one hundred neuronal receptor gene expression maps based on
73 transcriptional data from the Allen institute for brain science. In line with a specific activation
74 of the dopaminergic system, we found that both interventions predominantly activated
75 regions with high expression levels of the dopamine receptors D2 and D3.

76

77

78

79

80

81

82

Significance Statement

Studies in animals and humans provide evidence that transcranial direct current stimulation (tDCS) allows a manipulation of the dopaminergic system. Based on these findings, we used functional magnetic resonance imaging (fMRI) to assess changes in spontaneous neural activity strength in the human dopaminergic system after prefrontal tDCS in comparison to the administration of the dopamine precursor and standard anti-Parkinson drug levodopa (L-DOPA). We found that prefrontal tDCS and L-DOPA both enhance neural activity in core regions of the dopaminergic system and show similar subcortical activation patterns. Using whole-brain transcriptional data of more than one hundred neuronal receptor genes, we found that both interventions specifically activated regions with high expression levels of the dopamine receptors D2 and D3.

111 Introduction

112 The functional diversity of the dopaminergic system explains the close relationship between
 113 dopamine dysfunctions and a multifaceted range of neuropsychiatric disorders, including
 114 Parkinson's disease (PD), addiction, and schizophrenia (Kalivas and Volkow, 2005; Goto and
 115 Grace, 2007; Galvan and Wichmann, 2008). Thus, therapeutic strategies for manipulating
 116 dopaminergic system activity are of great clinical relevance, but, despite major advances,
 117 they are frequently accompanied by sometimes severe side effects (Katzenschlager and
 118 Lees, 2002; Foster and Hoffer, 2004; Appleby et al., 2007).

119
 120 There is now increasing evidence from studies in animals and humans that transcranial
 121 direct current stimulation (tDCS) might be an effective non-pharmacological and non-invasive
 122 way to activate deep brain regions of the dopaminergic system. tDCS is a form of sub-
 123 threshold brain stimulation that is based on a weak constant current, applied between an
 124 anodal and a cathodal electrode both placed on the scalp. Anodal stimulation causes the
 125 resting membrane potential to become slightly more positive, whereas cathodal stimulation
 126 slightly hyperpolarises the membrane. Hence, rather than causing neurons to fire, tDCS is
 127 supposed to modulate their excitability (Nitsche and Paulus, 2000; Rahman et al., 2013).

128
 129 Takano et al. (2011) combined tDCS with fMRI in rats and observed increased fMRI signal
 130 intensities in the nucleus accumbens (NAcc) after anodal stimulation over the frontal cortex.
 131 Using the same electrode placement, Leffa et al. (2016) found elevated striatal dopamine
 132 levels after tDCS. Moreover, Lu et al. (2015) showed that anodal tDCS over the frontal cortex
 133 not only increased whole-brain dopamine levels but also relieved symptoms in a mouse
 134 model of PD, comparable in effect to L-DOPA, a standard anti-PD drug, which is converted
 135 to dopamine in the intracellular space of dopaminergic midbrain neurons (Volkow et al.,
 136 1996).

138 Several studies in humans have already demonstrated effects on neural activity in striatal
 139 areas during and after tDCS over prefrontal and motor cortical areas (Polanía et al., 2012;
 140 Chib et al., 2013; Hone-Blanchet et al., 2016) and a recent study provided first molecular
 141 evidence of elevated striatal dopamine levels after prefrontal tDCS in humans (Fonteneau et
 142 al., 2018). Based on these results, we examined the enhancement of neural activity in
 143 regions of the dopaminergic system before and after prefrontal tDCS and compared the
 144 effect to a pharmacological stimulation of dopamine synthesis.

145
 146 We conducted two separate resting-state fMRI (rsfMRI) studies in healthy humans. In the
 147 first study (tDCS study), we applied a tDCS protocol developed by Chib et al. (2013), who
 148 provided first evidence for a causal manipulation of distant dopaminergic brain regions and
 149 associated dopamine-dependent functions after anodal stimulation over the
 150 frontopolar/ventromedial prefrontal cortex (fp/vmPFC, 10-20 electrode system: Fpz) and
 151 cathodal stimulation over the right dorsolateral prefrontal cortex (dlPFC, F4). In a parallel
 152 study design, we used the anodal/cathodal Fpz/F4 montage in the experimental group (main,
 153 n=20) and the same electrode locations but inverse polarity in a control group (inverse,
 154 n=20). We examined the fractional amplitudes of low-frequency signal fluctuations (fALFF), a
 155 proxy of spontaneous neural activity strength (Zou et al., 2008), in subcortical regions of the
 156 dopaminergic system before and after prefrontal tDCS. The same analysis was performed in
 157 a second study (L-DOPA study, n=22), in which the effect of a single dose of L-DOPA versus
 158 placebo was examined in a cross-over design.

159
 160 The effect of tDCS and L-DOPA on fALFF was examined in a dopaminergic system mask
 161 and fALFF changes in predefined subcortical regions (subcortical activation profiles) were
 162 compared between both interventions. We furthermore compared tDCS- and L-DOPA-
 163 induced whole-brain activity patterns with >100 neuronal receptor gene expression maps,
 164 based on transcriptional data from the Allen institute for brain science, to assess similarities

between the interventions in receptor-specific activation patterns and to analyse the relative specificity for regions with high dopamine receptor expression.

To support L-DOPA-induced fALFF changes in the dopaminergic system from a cross-species perspective, we also report results from a study in which we analyzed fALFF in the dopaminergic system of medetomidine sedated rats (n=6).

Materials and Methods

Experimental Design and Statistical Analysis

Procedures tDCS study (humans). 42 healthy participants were enrolled. The Ethics Committee of the State Medical Board in Rheinland-Pfalz, Germany, approved the study, and all participants gave written informed consent. Regular use of illegal drugs was an exclusion criterion. Two participants were excluded due to technical problems (n=40).

In a single-blind parallel study design, participants were randomly assigned to the main (n=20, 11 females, mean age: 25.7 years, age range: 21-32 years) or the inverse group (n=20, 11 females, mean age: 25.1 years, age range: 19-32 years). There was no significant age difference between the groups ($t_{38}=0.57$, $p=0.573$, two-tailed t -test). rsfMRI data were acquired before (pre) and ~5min after (post) tDCS application. Prior to the first rsfMRI measurement, electrode positions were marked on the participant's head to allow a fast electrode placement after the first scan. The 10-20 international system for electroencephalography was used for electrode positioning. We employed a tDCS protocol developed by Chib et al. (2013) and placed a 3.5 cm x 3.5 cm (12.25 cm²) anode with its center over electrode position Fpz and a 5 cm x 5 cm (25 cm²) cathode over electrode position F4 in the main group. Using this specific protocol, Chib et al. were able to modulate

193 fronto-midbrain interactions and reported a correlation between tDCS-induced neural effects
 194 and reward-related behavioral changes. Hence, the authors found evidence for a causal
 195 manipulation of distant dopaminergic brain regions and associated dopamine-dependent
 196 functions. For the control condition, we also followed Chib et al., who, after an extensive
 197 series of testing, selected an active control condition with maximum similarity to the
 198 experimental condition in which the same electrode placement was used with inverse
 199 polarity. The electric field distribution was simulated using the SimNIBS software package
 200 (Thielscher et al., 2015).

201

202 tDCS was applied using a battery-driven constant-current stimulator (DC-Stimulator,
 203 neuroConn GmbH, Ilmenau, Germany). Constant current was delivered for 15 min at 2 mA
 204 intensity (20 s ramp in and 20 s ramp out) through conductive rubber electrodes inserted into
 205 saline-soaked sponge pockets. Controlled by the DC-Stimulator, the impedance was kept <
 206 10 kΩ.

207

208 **Procedures L-DOPA study (humans).** 24 healthy male participants were enrolled.
 209 Participation was restricted to male participants because of potential estrogen-dopamine
 210 interaction effects on brain activity (Sánchez et al., 2012). A board-certified physician
 211 screened participants for contraindications of L-DOPA intake. Participants who reported to
 212 take illegal drugs on a regular basis were excluded. Abuse of illegal drugs was tested by
 213 urine drug screen (M10/3-DT; Diagnostik Nord). Participants were asked about their smoking
 214 habits but only three participants were smokers (each <5 cigarettes/day). The Ethics
 215 Committee of the State Medical Board in Rheinland-Pfalz, Germany, approved the study and
 216 all participants gave written informed consent. Two participants were excluded from rsfMRI
 217 analyses due to head motion and severe tiredness. Head motion was assessed based on
 218 realignment parameters (see rsfMRI data preprocessing [humans]) and tiredness was
 219 assessed by monitoring the right eye of the participant using an MRI-compatible camera (MR
 220 Cam Model 12M; MRC Systems, Germany). Participants who closed their eyes continuously

221 or repeatedly for more than ~5 sec during rsfMRI scans were excluded. Eventually, rsfMRI
 222 data from 22 participants were analyzed (mean age: 29.3 years, age range: 25-39 years).

223

224 rsfMRI data were acquired on two measurement days (day 1 and 2), separated by at least 5
 225 and not more than 14 days (Damoiseaux et al., 2006). In a cross-over design, each
 226 participant received either L-DOPA at day 1 followed by a placebo treatment at day 2 or vice
 227 versa. A third person randomly assigned participants to one of the two treatment sequences.
 228 Experimenter and participants were both blinded. Participants were told not to eat 1.5 h prior
 229 to the L-DOPA / placebo intake. Drugs were administered orally as capsules of 150 mg of L-
 230 DOPA with 37.5 mg benserazide (Levodopa-Benserazid-ratiopharm®, Germany) or an
 231 identically looking placebo capsule filled with mannitol and aerosil. Drugs were prepared and
 232 provided by the pharmacy of the University Medical Center Mainz. On both days, L-
 233 DOPA/placebo administration was directly followed by an rsfMRI baseline measurement at
 234 which no L-DOPA effect can be expected (LD_{0min}/Plc_{0min}). Further rsfMRI scans were
 235 performed after 45 (LD_{45min}/Plc_{45min}) and 90 min (LD_{90min}/Plc_{90min}), to capture the approximate
 236 times of maximum L-DOPA plasma concentration (Benetello et al., 1997; Hilal-Dandan and
 237 Brunton, 2014). Comparable time points have been chosen in other studies examining the
 238 effect of L-DOPA on resting state activity (Flodin et al., 2012; Cole et al., 2013; Haaker et al.,
 239 2013). Participants stayed under medical observation for the duration of the experiment,
 240 including heart rate and blood pressure measurements and questionnaires on potential side
 241 effects.

242

243 **Procedures L-DOPA study (rats).** In an additional animal rsfMRI study, we tested the effect
 244 of L-DOPA on mesostriatal fALFF values in rats. Female Lewis rats ($n=6$; >12 weeks old;
 245 160–180 g) were used in this experiment due to their limited growth in comparison to males.
 246 Each animal was scanned under placebo (NaCl, 0.9%) and L-DOPA. The order was
 247 randomized and the time interval between both measurements was at least one week.
 248 Animals were anesthetized with isoflurane 1.5% (Forene, Abbott, Wiesbaden, Germany)

249 during the scanner placement procedure. Temperature and breathing rate were monitored
 250 during the entire experiment by an MRI compatible monitoring system (SA Instruments, NY,
 251 USA). After the placement of the animal and the intraperitoneal injection of L-DOPA (10
 252 mg/kg)+benzeraside (20 mg/kg) or placebo, a bolus of 0.04 mg/kg of medetomidine was
 253 administrated in order to obtain a persistent state that shows neuronal and BOLD activity that
 254 resembles the awake state (Schwalm et al., 2017). We confirmed the persistent brain states
 255 based on an additional scan applying visual stimuli, yielding localized activation of the
 256 primary visual cortex, in sharp contrast to the cortex-wide activation in slow wave state. Five
 257 minutes later, isoflurane anesthesia was turned off and medetomidine 0.08 mg/kg/h was
 258 perfused until the end of the experiment. rsfMRI scans were performed 45, 60, 75, 90 and
 259 120 min after L-DOPA/ placebo administration in line with previous rodent studies showing
 260 that striatal dopamine peaks between 60 and 90 min after L-DOPA administration (Fornai
 261 et al., 1999).

262
 263 **fALFF analysis (humans and rats).** The amplitude of low-frequency fluctuations (ALFF) of
 264 the rsfMRI signal has been introduced to assess the intensity of regional spontaneous brain
 265 activity in humans (Zang et al., 2007). To reduce the sensitivity to physiological noise, Zou et
 266 al. (2008) developed fractional ALFF (fALFF), which is defined as the ratio of the low-
 267 frequency amplitudes (0.01–0.08 Hz) to the amplitudes of the entire frequency range (0–0.25
 268 Hz). In humans, fALFF analyses on preprocessed rsfMRI data were performed using the
 269 REST toolbox (Zang et al., 2007). In rats, the same frequencies were analyzed using an in-
 270 house matlab script (The Mathworks, Inc., Natick, MA). Since small changes in anesthesia
 271 levels can modify dramatically the amplitude of low frequency fluctuations in rats (Maandag
 272 et al., 2007), the obtained values were then normalized by the mean fALFF of the cortical and
 273 subcortical structures.

274
 275 **ROI analysis (humans).** To test our a priori hypothesis of dopaminergic system activation,
 276 ROI analyses in humans were performed for a combined bilateral dopaminergic system

mask (including the nucleus accumbens [Nacc], caudate [Caud], putamen [Put], substantia nigra [SN] and the ventral tegmental area [VTA]). NAcc, Caud and Put masks were created based on the HO (Harvard Oxford) brain atlas (Frazier et al., 2005; Desikan et al., 2006; Makris et al., 2006; Goldstein et al., 2007) using a tissue probability cut-off threshold of 50%. The SN and the VTA were combined in a single previously published mask (Bunzeck and Düzel, 2006; Düzel et al., 2009).

283

In the tDCS and the L-DOPA study in humans, fALFF values of voxels within the dopaminergic system mask were averaged and analyzed in a repeated measures ANOVA using SPSS (Version 23). In the tDCS study, stimulation group (main, inv) and time (pre, post) were entered as between-subject and within-subject factors, respectively. In the L-DOPA study, both treatment and time (0 min, 45 min and 90 min after drug administration) were entered as within-subject factors. Partial eta-squared values (η_p^2) are reported as effect size measures. ANOVA results were further characterized by Bonferroni-corrected post hoc two-tailed *t*-tests (tDCS study: post- vs. pre-tDCS in both groups; L-DOPA study: 45 vs. 0 min, 90 vs. 0 min in both conditions). Bonferroni-corrected *p*-values are denoted as p_{Bonf} . p_{Bonf} values greater than 1 are reported as $p_{\text{Bonf}}=1$.

294

A potential baseline difference between the main and the inverse group in the tDCS study and between the L-DOPA and placebo condition in the L-DOPA study was tested by two-tailed *t*-tests. Gender-related effects in the tDCS study were tested by adding gender as between-subject factor to the repeated measures ANOVA. In the L-DOPA study, effects related to treatment order were tested by adding treatment order as between-subject factor.

300

A spectral analysis of mesostriatal rsfMRI time courses was performed in the tDCS and in the human L-DOPA study using the REST toolbox (Zang et al., 2007) to inspect if non-resting state frequencies were affected by the two manipulations. For each subject, power spectra were calculated from unfiltered time courses of voxels within the dopaminergic

305 system mask. Next, power spectra were averaged across voxels, smoothed by a moving
 306 average and finally normalized.

307

308 **ROI analysis (rats).** A mask, covering the entire striatum and the SN was applied as
 309 dopaminergic system mask in the L-DOPA rat study using the atlas template from Valdés-
 310 Hernández et al. (2011). Averaged fALFF values were analyzed in a repeated measures
 311 ANOVA with treatment and time (45 min, 60 min, 75 min and 90 min after drug
 312 administration) as within-subject factors using SPSS (Version 23). Significant effects were
 313 further characterized by means of two-tailed *t*-tests (uncorrected).

314

315 **Voxel-wise analysis (humans).** To investigate the anatomical distribution of fALFF effects
 316 within the human dopaminergic system, voxel-wise analyses were performed for each
 317 subregion of the dopaminergic system mask (bilateral NAcc, Put, Caud and the SN/VTA)
 318 using the MatLab toolbox Statistical Parametric Mapping 8 (SPM8, Wellcome Trust Centre
 319 for Neuroimaging, UK). fALFF values were entered into a group analysis using SPM's flexible
 320 factorial design. In the tDCS study, stimulation group and time were entered as between-
 321 subject and within-subject factors, respectively. In the L-DOPA study, both treatment and
 322 time were entered as within-subject factors. tDCS-induced activation in the main as
 323 compared to the inverse group was tested by the following contrast: $[tDCS_{main,post} -$
 324 $tDCS_{main,pre}] > [tDCS_{inv,post} - tDCS_{inv,pre}]$. To test for L-DOPA-induced effects after 45 and 90
 325 min, the following contrasts were calculated: 45 min = $[LD_{45min} - LD_{0min}] > [Plc_{45min} - Plc_{0min}]$,
 326 90 min = $[LD_{90min} - LD_{0min}] > [Plc_{90min} - Plc_{0min}]$. Baseline differences between the tDCS groups
 327 and the L-DOPA / placebo condition were tested in all subregions of the dopaminergic
 328 system in both directions ($tDCS_{main,pre} > tDCS_{inv,pre}$, $tDCS_{main,pre} < tDCS_{inv,pre}$; $LD_{0min} > Plc_{0min}$,
 329 $LD_{0min} < Plc_{0min}$). Family-wise error (FWE) correction was performed for voxel-level inference
 330 as implemented in SPM8 at a threshold of $\alpha = 0.05$ for each region (SVC = small-volume
 331 correction).

332 In both studies, the peak voxel cluster was further characterized by a functional connectivity
 333 (FC) analysis. FC-maps were z-transformed and analyzed on a whole brain level using
 334 SPM's flexible factorial design (see above for contrasts).

335

336 **Analysis of subcortical activation profiles (humans).** To examine tDCS- and L-DOPA-
 337 induced effects in single subregions of the dopaminergic system (bilateral NAcc, Put and
 338 Caud) and to test if subcortical regions that are not part of the predefined dopaminergic
 339 system mask (bilateral hippocampus, amygdala, thalamus, pallidum and the brainstem) were
 340 significantly affected, we analyzed changes in averaged fALFF values for the entire set of 15
 341 subcortical grey matter HO atlas regions. tDCS- and L-DOPA-related activation was
 342 analyzed by means of Bonferroni-corrected two-tailed *t*-tests (tDCS: [tDCS_{main,post} -
 343 tDCS_{main,pre}] vs. [tDCS_{inv,post} - tDCS_{inv,pre}]; L-DOPA (45 min): [LD_{45min} - LD_{0min}] - [Plc_{45min} -
 344 Plc_{0min}]; L-DOPA (90 min): [LD_{90min} - LD_{0min}] - [Plc_{90min} - Plc_{0min}]). To assess the relationship of
 345 tDCS- and L-DOPA-induced subcortical activation profiles, corresponding effect sizes
 346 (Cohen's *d*) were calculated for each single region and compared between the two
 347 interventions by means of Pearson correlation (*r*, $\alpha=0.05$).

348

349 **Analysis of gene-fALFF similarity profiles (humans).** We compared uncorrected group-
 350 level statistical parametric maps (*t*-maps) resulting from voxel-wise analyses with gene
 351 expression maps based on transcriptional data from the Allen institute for brain science (AIB)
 352 (Hawrylycz et al., 2012). Our aim was to examine similarities between brain activation maps
 353 and different neuronal receptor gene expression patterns, including those of the dopamine
 354 receptors D1-D5 (DRD1-DRD5). The AIB provides whole-brain-sampled transcriptional data
 355 of over 20000 genes based on six post-mortem brains. Averaged and smoothed (6 mm hard
 356 sphere) AIB gene expression maps were available from the Neurosynth database (Yarkoni et
 357 al., 2011). We restricted our analysis to genes encoding receptors of eleven preselected
 358 neurotransmitters and neuromodulatory ligands, resulting in a total number of 115 genes
 359 (adrenergic receptors: ADRA1A, ADRA1B, ADRA1D, ADRA2A-C, ADRB1-3; cholinergic

360 receptors: CHRM1-5, CHRNA1-5, CHRNA7-10, CHRNB1-4, CHRND, CHRNE, CHRNG;
 361 cannabinoid receptors: CRN1, CRN2; corticotropin releasing hormone receptors: CRHR1,
 362 CRHR2; dopamine receptors: DRD1-5; GABA receptors: GABARAP, GABBR1, GABBR2,
 363 GABARAPL1, GABARAPL2, GABRA1-6, GABRB1-3, GABRD, GABRE, GABRG1-3,
 364 GABRP, GABRQ, GABRR1-3; glutamate receptors: GRIA1-4, GRID1-2, GRIK1-5, GRIN1,
 365 GRIN2A-D, GRIN3A-B, GRINA, GRIP1-2, GRM1-8; 5-hydroxytryptamine receptors: HTR1A-
 366 B, HTR1D-F, HTR2A-C, HTR3A-E, HTR4, HTR5A, HTR6-7; glucocorticoid receptor: NR3C1;
 367 BDNF receptor: NTRK2; opioid receptors: OPRD1, OPRK1, OPRL1, OPRM1). Pearson
 368 correlations were calculated between *t*-maps ($tDCS$: [$tDCS_{main,post} - tDCS_{main,pre}$] > [$tDCS_{inv,post}$
 369 - $tDCS_{inv,pre}$]; L-DOPA: [$LD_{45min} - LD_{0min}$] > [$Plc_{45min} - Plc_{0min}$], 90 min = [$LD_{90min} - LD_{0min}$] >
 370 [$Plc_{90min} - Plc_{0min}$]) and gene expression maps. *t*-values of different voxels with the same gene
 371 expression intensity were averaged so that each unique gene expression intensity value was
 372 paired with a single averaged *t*-value in the correlation analysis. For each contrast we
 373 obtained a profile of correlation coefficients, indicating similarities between the induced
 374 fALFF pattern and 115 gene expression patterns (gene-fALFF similarity profile = GFS
 375 profile). GFS profiles were z-transformed and compared between the two studies using
 376 Pearson correlations (*r*, $\alpha=0.05$) to analyse to what extent both interventions showed
 377 comparable receptor-specific activation patterns. To furthermore assess the relative
 378 specificity for dopaminergic target regions, we determined for both interventions the
 379 percentage of genes showing higher z-scores than a specific dopamine receptor gene (i.e., a
 380 small percentage indicates a high specificity). The analysis was performed for all dopamine
 381 receptors (DRD1-DRD5).

382

383 **Data recording and processing**

384 **rsfMRI data recording (humans).** In humans, rsfMRI data were obtained with a 3 Tesla MR
 385 scanner (MAGNETOM Trio; Siemens, Germany) by using a 32-channel head coil. Blood
 386 oxygenation-level dependent (BOLD) signal was acquired using a T2*-sensitive gradient
 387 echo-planar imaging (EPI) sequence with simultaneous multislice (SMS) acquisition

technique (TR: 1.0 s; TE: 29 ms; multiband acceleration factor: 4; field of view: 210×180 mm; 2×2 mm in-plane resolution). Each 3D-image comprised 60 contiguous axial slices (2.5 mm thick). The position of the slice package was individually adjusted for whole-brain image acquisition. Participants were instructed to remain awake with their eyes open. A fixation cross was presented on the screen center during scans. Time series of 600 rsfMRI images were acquired per session (10 min) in the tDCS study and 480 rsfMRI images per session (8 min) in the L-DOPA study. To account for T1 equilibrium effects, the first five images of each time series were discarded. This resulted in 595 and 475 rsfMRI images per session for the tDCS and the L-DOPA study, respectively. At the end of the experiment, a high-resolution T1-weighted structural image was further acquired.

rsfMRI data preprocessing (humans). rsfMRI data were preprocessed using SPM8. Preprocessing of the rsfMRI data first involved realignment to correct for head movements. rsfMRI data were then coregistered with corresponding T₁-weighted anatomical images and normalized to a standard template from the Montreal Neurological Institute (MNI) in order to allow for group comparisons. Finally, rsfMRI data were spatially smoothed with a 6 mm full-width-at-half-maximum (FWHM) isotropic Gaussian kernel. Participants showing head displacements greater than 2.5 mm (slice thickness; values were extracted from realignment parameters) were excluded. To further correct for possible effects of movement and other systemic effects, the six movement parameters resulting from realignment and mean cerebrospinal fluid (CSF) and white matter (WM) time series were regressed out.

Mean framewise displacements (humans). We analyzed mean framewise displacements (Power et al., 2012) to test if tDCS and L-DOPA had specific effects on head movement and if head movement differed between tDCS groups. Mean framewise displacements were calculated from movement parameters and analyzed in repeated measures ANOVAs (tDCS: stimulation x time interaction; L-DOPA: treatment x time interaction; see ROI analysis for a detailed description of the ANOVA design).

rsfMRI data recording and preprocessing (rats). rsfMRI data acquisition was performed on a 9.4 T small animal imaging system with a 0.7 T/m gradient system (Biospec 94/20, Bruker Biospin GmbH, Ettlingen, Germany). For rsfMRI measurements, T2*-weighted images were acquired with a single-shot gradient EPI sequence with TR = 1.5 s, TE = 14 ms, FA 65°, 320 × 290 μm, slice thickness 0.8 mm. Altogether, 600 images, each comprising 34 contiguous slices, were acquired per scan, resulting in a scan time of 15 min. Each scan of 600 images was preprocessed using Brain Voyager QX (vs. 2.8.4, Brain innovation, Maastricht, The Netherlands). rsfMRI data were realigned to correct for head movements and smoothed with a 0.7 mm FWHM isotropic gaussian kernel. Using the same software, rsfMRI data were manually aligned to a T1 template from (Valdés-Hernández et al., 2011) containing 150 cortical and subcortical regions. Finally, a high-resolution T1-weighted structural image (0.125×0.125×0.125mm) was acquired.

Results

Side effect reports and mean framewise displacements. All participants of the tDCS study reported a mild tingling under the electrodes during stimulation, irrespective of the group. However, no other somatic or psychological side effects that were attributable to the intervention were reported. Likewise, no treatment-related side effects were reported in the L-DOPA study. Analyzing mean framewise displacements revealed that tDCS and L-DOPA had no specific effects on head movement (tDCS: stimulation x time interaction: $F_{1,38}=1.28$, $p=0.264$; L-DOPA study: treatment x time interaction: $F_{2,42}=0.7$, $p=0.503$) and there was also no significant difference between tDCS groups ($F_{1,38}=0.65$, $p=0.426$).

Electric field simulation (tDCS study). A simulation of the electric field (anode: Fpz, cathode: F4) indicated maximal electric field strength (~0.3 V/m) in the right superior and middle frontal gyrus (Figure 1). Field strengths were comparable to those generated by other

443 prefrontal montages (see e.g. Saturnino et al., 2015) suggesting that a substantial amount of
 444 current passed through cortical areas.

445

446 **ROI analysis (tDCS study).** We first tested our a priori hypothesis that stimulation in the
 447 main group remotely activates brain areas of the subcortical dopaminergic system as
 448 compared to stimulation with inverse polarity. When averaging across voxels in a
 449 dopaminergic system mask (Figure 2A), we found significant main effects of time
 450 ($F_{1,38}=22.16$, $p<0.001$, $\eta_p^2=0.37$) and stimulation ($F_{1,38}=7.3$, $p=0.01$, $\eta_p^2=0.16$), which however
 451 could be explained by a significant stimulation x time interaction ($F_{1,38}=13.77$,
 452 $p<0.001$, $\eta_p^2=0.266$; Figure 2B). A strong fALFF increase in the main as opposed to the
 453 inverse tDCS group from pre to post stimulation was supported by post hoc *t*-tests (main:
 454 $t_{19}=5.08$, $p_{\text{Bonf}}<0.001$; inv: $t_{19}=0.89$, $p_{\text{Bonf}}=0.77$). Power spectra, calculated from time courses
 455 of masked mesostriatal voxels, indicated that tDCS most strongly amplified classical resting-
 456 state frequencies ranging from 0.01 to 0.08 Hz (Figure 3A).

457

458 There was no significant fALFF difference between the two groups at baseline ($t_{38}=-1.22$,
 459 $p=0.231$) and no significant effects of gender were found (main effect of gender: $F_{1,36}=0.68$,
 460 $p=0.416$; time x stimulation x gender interaction: $F_{1,36}=0.22$, $p=0.642$).

461

462 **ROI analysis (L-DOPA study in humans).** We found a significant treatment x time
 463 interaction indicating an L-DOPA-induced fALFF increase in the dopaminergic system
 464 ($F_{2,42}=4.17$, $p=0.022$, $\eta_p^2=0.166$; Figure 2C). The interaction subsumed a main effect of time
 465 ($F_{2,42}=5.34$, $p=0.009$, $\eta_p^2=0.20$). Post hoc *t*-tests revealed a significant fALFF increase 90 min
 466 but not 45 min after L-DOPA administration (90 min: $t_{21}=4.35$, $p_{\text{Bonf}}<0.001$; 45 min: $t_{21}=1.17$,
 467 $p_{\text{Bonf}}=1$). fALFF increases after placebo administration were not supported (90 min: $t_{21}=0.66$,
 468 $p_{\text{Bonf}}=1$; 45 min: $t_{21}=0.48$, $p_{\text{Bonf}}=1$). As for tDCS, the spectral power analysis supported major
 469 effects on resting-state frequencies (Figure 3B).

470

471 Treatment order had no significant effect on fALFF values (main effect: $F_{1,20}=0.02$, $p=0.878$,
 472 treatment x time x order interaction: $F_{2,40}=1.96$, $p=0.154$). There was no significant difference
 473 between the two conditions at baseline ($t_{21}=0.95$, $p=0.354$).

474

475

476 **ROI analysis (L-DOPA study in rats).** In an additional L-DOPA study, we conducted a
 477 comparable experimental approach in rats, masking the homologous brain regions, with
 478 recordings performed at 45, 60, 75, 90 and 120 minutes after L-DOPA / placebo
 479 administration. As in the human studies, we performed a ROI analysis on averaged fALFF
 480 values and found that L-DOPA led to a significant fALFF increase that reached its peak after
 481 45 to 75 min (treatment x time interaction: $F_{4,20}=3.62$, $p=0.023$, $\eta_p^2=0.43$; Figure 4).

482

483 **Voxel-wise analysis (tDCS study).** Examining the voxel-wise spatial distribution of tDCS-
 484 induced effects within subregions of the dopaminergic system revealed significant activations
 485 in multiple striatal areas, including the bilateral Caud, NAcc, Put and the SN/VTA (Table 1).
 486 The right Put showed the strongest activation cluster, which was mainly located in dorsal
 487 parts of the striatum (Figure 5). None of the mesostriatal regions showed a baseline
 488 difference between the groups.

489

490 Extending the analysis of tDCS-induced effects to other subcortical HO atlas regions
 491 (bilateral hippocampus, amygdala, thalamus, pallidum and the brainstem) showed no further
 492 significant results and no significant FC changes were found for the right Put (peak voxel
 493 cluster).

494

495 **Voxel-wise analysis (L-DOPA study in humans).** In contrast to the analysis of averaged
 496 fALFF values, voxel-wise analyses revealed a significant activation 45 min after L-DOPA
 497 administration that was restricted to the SN/VTA. After 90 minutes, L-DOPA-induced effects
 498 were found in ventral parts of the striatum, where the strongest activation was observed at

the borderline between the left NAcc, Caud and Put (Table 2 and Figure 5). None of the mesostriatal regions showed a significant baseline difference.

501

An exploratory analysis of all subcortical HO atlas regions furthermore indicated L-DOPA-induced activations after 90 min in the brainstem (x,y,z: 6,-38,-44; $p_{FWE}=0.009$, SVC), left pallidum (x,y,z: -24,-12,0; $p_{FWE}=0.028$, SVC), left thalamus (x,y,z: -12,-28,12; $p_{FWE}=0.027$, SVC) and the left amygdala (x,y,z: -30,6,-22; $p_{FWE}=0.049$, SVC). No further activations were found when analyzing the time window 45 minutes after treatment administration. The ventral striatum peak cluster showed a significant L-DOPA-induced FC increase with the right cerebellum after 90 min (x,y,z: 38,-52,-32; $p_{FWE}=0.026$, whole-brain analysis). No significant L-DOPA-induced FC changes were found for the SN/VTA in the time window 45 min after treatment administration.

511

Analysis of subcortical activation profiles. We examined tDCS-induced activity changes (for each subcortical HO atlas region) on a region-wise anatomical scale and again found peak activations in key regions of the mesostriatal dopamine system. The right and left Put and Caud constituted the four most activated subcortical brain regions, of which the Put on both sides reached the level of Bonferroni-corrected statistical significance ($[tDCS_{main,post} - tDCS_{main,pre}]$ vs. $[tDCS_{inv,post} - tDCS_{inv,pre}]$; right Put: $t_{38}=3.93$, $p_{Bonf}=0.005$; left Put: $t_{38}=3.17$, $p_{Bonf}=0.045$). In the L-DOPA study, the right and left Caud constituted the most activated subcortical brain regions 90 min after L-DOPA intake, of which the latter reached the level of Bonferroni-corrected statistical significance ($[LD_{90min} - LD_{0min}] - [Plc_{90min} - Plc_{0min}]$; $t_{21}=3.37$, $p_{Bonf}=0.045$). No significant activation was found 45 minutes after L-DOPA administration.

522

To compare subcortical activation profiles of both interventions, we next calculated effect sizes (Cohen's d) for all subcortical HO atlas regions. No significant relationship was found when comparing the effect size profiles for L-DOPA after 45 minutes with tDCS ($r=-0.19$, $p=0.504$). However, there was a significant correlation when comparing the profiles for L-

527 DOPA after 90 minutes and tDCS ($r=0.73$, $p=0.002$; Figure 6) suggesting a potential analogy
 528 of tDCS- and L-DOPA-induced subcortical effects.

529

530 **Analysis of gene-fALFF similarity profiles.** We finally calculated correlations between
 531 tDCS-/L-DOPA-related brain activation maps (uncorrected whole-brain t -maps resulting from
 532 voxel-wise analyses) and 115 receptor gene expression patterns (GFS profiles) to examine
 533 the relative specificity of both interventions for regions with high dopamine receptor
 534 expression and to compare GFS profiles between the two interventions. z -transformed GFS
 535 profiles showed a strong correlation indicating that tDCS and L-DOPA activated brain regions
 536 with similar receptor composition (tDCS vs. L-DOPA (90 min): $r=0.88$, $p<0.001$; tDCS vs. L-
 537 DOPA (45 min): $r=0.82$, $p<0.001$; Figure 7).

538

539 Among all 115 preselected receptor genes, the DRD2 expression pattern most strongly
 540 resembled the activation pattern induced by tDCS and only 1.74% of the gene expression
 541 maps (i.e., two gene expression maps) correlated more with the tDCS-induced activation
 542 pattern than the DRD3 expression map (DRD2 and the epsilon subunit of the GABA A
 543 receptor [GABRE]). DRD2 and DRD3 expression maps also showed a strong correlation with
 544 the L-DOPA-induced pattern after 90 min in comparison to other genes: As for tDCS, no
 545 other gene expression map showed a stronger correlation than DRD2 and only four gene
 546 expression maps (3.48%) correlated more with the L-DOPA-induced pattern than DRD3
 547 (DRD2, 5-hydroxytryptamine receptor 1D [HTR1D], alpha-2B adrenergic receptor [ADRA2B],
 548 alpha-2C adrenergic receptor [ADRA2C]; Figure 7). Hence, both interventions showed a high
 549 similarity in their receptor-specific activation patterns and specifically activated regions with
 550 high DRD2 and DRD3 expression levels.

551

552 Analyzing the L-DOPA effect 45 min after administration revealed that 5.21% and 7.83% of
 553 all gene expression maps showed a stronger correlation with the brain activation pattern than
 554 DRD2 and DRD3, respectively. In contrast to DRD2 and DRD3, other dopamine receptor

expression maps showed less similarity with tDCS- and L-DOPA-induced patterns, i.e., more genes showed stronger correlations (tDCS: DRD1=14.78%, DRD4=75.65%, DRD5=33.04%; L-DOPA (45 min): DRD1=40.87%, DRD4=60.87%, DRD5=51.3%; L-DOPA (90 min): DRD1=8.7%, DRD4=49.57%, DRD5=57.39%). The difference between DRD2-3 on the one hand and DRD1 and DRD4-5 on the other was also reflected when analyzing correlations between the gene expression maps of the dopamine receptors indicating the strongest correlation between DRD2 and DRD3 ($r=0.67$, Table 3).

Discussion

We tested the influence of prefrontal tDCS and L-DOPA on deep regions of the mesostriatal dopamine system at rest in healthy humans. Regional neural activity strength was assessed by means of fALFF analyses. Anodal/cathodal Fpz/F4 stimulation led to enhanced fALFF values in key regions of the dopaminergic system. No effects were observed when the same montage was used with inverse polarity. Increased activity in mesostriatal regions was also found after L-DOPA administration. Both interventions showed distinct similarities in subcortical and receptor-specific activation profiles, suggesting mechanistic commonalities and a potential application of prefrontal tDCS in the treatment of dopamine dysfunctions.

To achieve better comparability between studies in animals and humans, we investigated fALFF in task-free resting states. fALFF has been applied as a proxy measure of spontaneous neural activity strength and has been used increasingly as a biomarker of neuropsychiatric diseases, including Alzheimer's disease (Zhou et al., 2015), schizophrenia (Xu et al., 2015) and depression (Liu et al., 2016). Several studies reported significant correlations of fALFF values and symptom severity in patients (Chen et al., 2015; Fryer et al., 2015) as well as behavioral performance in healthy humans (van Dam et al., 2015), suggesting a close association between resting-state fALFFs and specific behavioral parameters.

583

584 We employed a stimulation protocol developed by Chib et al. (2013) to remotely activate
 585 reward-related regions of the dopaminergic system. Chib et al. found increased task-related
 586 fMRI signal interactions between the vmPFC and the ventral midbrain after tDCS, and most
 587 importantly, participants with more enhanced fronto-midbrain interactions assigned higher
 588 attractiveness ratings when judging the attractiveness of computer-generated faces. These
 589 results indicated, for the first time, a tDCS-induced effect on midbrain parts of the
 590 dopaminergic system with direct behavioral consequences. However, an interpretation of
 591 Chib et al.'s results from a translational perspective is not straightforward, mainly because
 592 the authors investigated the effect of tDCS on reward-related brain activity in a task, which is
 593 only suited for human subjects.

594

595 Considering the neuroanatomical literature, anodal stimulation of glutamatergic projections
 596 from the vmPFC to the mesostriatal system may have evoked the observed fALFF increases
 597 (see e.g. Hedreen and DeLong, 1991; Frankle et al., 2006; Haber and Knutson, 2010).
 598 However, the electric field simulation indicated maximal field strength in right lateral cortical
 599 regions suggesting furthermore a crucial role of inhibitory cathodal stimulation over the right
 600 dlPFC (F4) in the remote activation of mesostriatal regions. Interestingly, Chib et al. tested
 601 multiple electrode montages but only observed effects on dopamine-dependent functioning
 602 when placing the cathode at F4 and the anode at Fpz. Furthermore, Fonteneau et al. (2018)
 603 reported elevated striatal dopamine levels after cathodal F4 and anodal F3 stimulation.
 604 Hence, one could speculate that the right dlPFC exerts inhibitory control over the
 605 dopaminergic system, which can be deactivated through cathodal stimulation. However,
 606 overall the electric fields generated by anodal/cathodal Fpz/F4 stimulation (used here and by
 607 Chib et al., 2013) and anodal/cathodal F3/F4 stimulation (used by Fonteneau et al., 2018)
 608 differ, which is against the hypothesis that both configurations activate the same neural
 609 pathway (see e.g. Austin et al., 2016; Bikson et al., 2018 for electric field maps of
 610 anodal/cathodal F3/F4 stimulation). An alternative explanation for striatal effects after both

611 anodal/cathodal Fpz/F4 and anodal/cathodal F3/F4 stimulation is provided by FC analyses in
 612 humans, showing a topological relationship between distinct cortical networks and specific
 613 striatal subregions (Choi et al., 2012). Hence, two different tDCS protocols, modulating
 614 activity in different parts of the prefrontal cortex (and thus possibly in different cortical
 615 networks), may both affect the striatum but through different cortico-striatal pathways and
 616 targeting different striatal subregions.

617

618 When comparing our results to those of Fonteneau et al. (2018), it should also be mentioned
 619 that Fonteneau et al. reported significant changes in dopamine release 20-35 min after tDCS
 620 but not directly after stimulation as shown for fALFF in the present study. To fully investigate
 621 this difference, it will be required to directly compare acute and late mesostriatal effects
 622 between the two tDCS protocols using both positron emission tomography (PET) and fMRI.

623

624 L-DOPA is converted to dopamine in the intracellular space of dopaminergic neurons, which
 625 form the neuroanatomical basis of dopamine-dependent neuromodulation (Volkow et al.,
 626 1996), while as previously stated, the effect of prefrontal tDCS is likely mediated by cortico-
 627 subcortical projections. Both interventions induced similar subcortical activation profiles on a
 628 region-wise anatomical scale, but however voxel-wise fALFF analyses also revealed intra-
 629 regional differences. This is not necessarily contradictory since ascending dopaminergic
 630 projections (activated by L-DOPA) and descending cortical projections (activated by tDCS)
 631 may target different parts of the same anatomical region. From a clinical perspective, this
 632 constitutes in fact a promising finding, as it points to a complementary and more effective
 633 stimulation of the dopaminergic system by combining both interventions in the treatment of
 634 dopamine dysfunctions.

635

636 So far there are only limited insights into the effects of L-DOPA on resting state fALFFs as
 637 most studies primarily focused on changes in FC (see e.g. Cole et al., 2013). One exception
 638 is the study by Flodin et al. (2012), who investigated L-DOPA-related fALFF changes in a set

639 of cortical and subcortical ROIs, but did not find significant striatal effects. However, it should
 640 be mentioned that the authors employed a between subjects design and acquired data at
 641 only 1.5 Tesla, which might have reduced the sensitivity to detect fALFF changes.

642

643 Using transcriptional data from the AIB, we found that both interventions manipulated neural
 644 activity in dopaminergic target regions characterized by high DRD2 and DRD3 expression.
 645 Although the analysis of gene expression maps may partly bridge the gap between
 646 hemodynamic effects and molecular mechanisms, it is important to note that we do not
 647 provide direct evidence for tDCS/L-DOPA-induced dopaminergic neurotransmission, which
 648 can only be achieved with molecular imaging techniques. In particular, the combination of
 649 fMRI and PET will finally help to understand the relationship between fALFF increases and
 650 dopamine release.

651

652 In an additional study, we analyzed the effects of L-DOPA in lightly sedated rats, which
 653 resembled those in awake humans. fALFF increases followed different temporal
 654 characteristics as compared to humans, which however might be explained by several
 655 factors that are difficult to control, most importantly differences in administration routes,
 656 dosage, and metabolic rate. Recent rodent studies (Cha et al., 2016; Yan et al., 2017) as
 657 well as our own results support fALFF as a suitable marker of intrinsic brain activity changes
 658 in animals. Furthermore, it supports the notion, that a direct (back-)translation of a network
 659 manipulation yields homologous oscillatory activity, provided that the brain state of the
 660 animal is being carefully controlled (Schwalm et al., 2017).

661

662 Several methodological drawbacks of the present approach should be mentioned. In the
 663 tDCS study, both genders were tested, whereas either only male humans or female rats
 664 were tested in the L-DOPA studies. A careful control would have been conducive to the
 665 comparability of both interventions and might have given additional information. Although
 666 experimenter effects are unlikely to occur in task-free study designs, it should be mentioned

667 that the tDCS study was only single-blinded. In both studies, blinding efficacy was not
668 assessed, but none of the participants reported unexpected side effects or perceived
669 symptoms (apart from cutaneous sensations at the site of stimulation in both tDCS groups),
670 which at least reduces the risk of a significant experimental bias. Finally, our tDCS study
671 does not include a sham group to exclude unspecific time-dependent effects. However, we
672 assume that such effects only play a minor role as they were not observed in the inverse
673 group of the tDCS study and in the placebo condition of the L-DOPA study.

674
675 In summary, in line with animal studies and recent molecular imaging studies in humans, we
676 found spatially specific tDCS-related activity increases in subcortical parts of the
677 dopaminergic system, particularly in the striatum. tDCS and L-DOPA showed comparable
678 subcortical and receptor-specific activation profiles, suggesting mechanistic commonalities
679 between both manipulations. These results are promising in respect of restoring depleted
680 dopamine levels and may expand the repertoire of tDCS protocols that have been
681 successfully applied in therapeutic contexts (Brunoni et al., 2012; Kalu et al., 2012).
682 However, future studies, testing whether the approach presented here affects clinically
683 relevant neurochemical and, most importantly, behavioral parameters are required to finally
684 draw conclusions on its potential clinical value.

685
686
687
688
689
690
691
692
693
694

References

- Appleby BS, Duggan PS, Regenbreg A, Rabins PV (2007) Psychiatric and neuropsychiatric adverse events associated with deep brain stimulation: A meta-analysis of ten years' experience. *Mov Disord Off J Mov Disord Soc* 22:1722–1728.
- Austin A, Jiga-Boy GM, Rea S, Newstead SA, Roderick S, Davis NJ, Clement RM, Boy F (2016) Prefrontal Electrical Stimulation in Non-depressed Reduces Levels of Reported Negative Affects from Daily Stressors. *Front Psychol* 7:315.
- Benetello P, Furlanut M, Fortunato M, Pea F, Baraldo M (1997) Levodopa and 3-O-methyldopa in cerebrospinal fluid after levodopa-carbidopa association. *Pharmacol Res* 35:313–315.
- Bikson M et al. (2018) Rigor and reproducibility in research with transcranial electrical stimulation: An NIMH-sponsored workshop. *Brain Stimulat* 11:465–480.
- Brunoni AR, Nitsche MA, Bolognini N, Bikson M, Wagner T, Merabet L, Edwards DJ, Valero-Cabre A, Rotenberg A, Pascual-Leone A, Ferrucci R, Priori A, Boggio P, Fregni F (2012) Clinical Research with Transcranial Direct Current Stimulation (tDCS): Challenges and Future Directions. *Brain Stimulat* 5:175–195.
- Bunzeck N, Düzel E (2006) Absolute coding of stimulus novelty in the human substantia nigra/VTA. *Neuron* 51:369–379.
- Cha J, Kim ST, Jung WB, Han YH, Im GH, Lee JH (2016) Altered white matter integrity and functional connectivity of hyperacute-stage cerebral ischemia in a rat model. *Magn Reson Imaging* 34:1189–1198.
- Chen Y-C, Xia W, Luo B, Muthaiah VPK, Xiong Z, Zhang J, Wang J, Salvi R, Teng G-J (2015) Frequency-specific alternations in the amplitude of low-frequency fluctuations in chronic tinnitus. *Front Neural Circuits* 9 Available at: <http://www.ncbi.nlm.nih.gov/pmc/articles/PMC4624866/> [Accessed July 28, 2017].

- 720 Chib VS, Yun K, Takahashi H, Shimojo S (2013) Noninvasive remote activation of the ventral
721 midbrain by transcranial direct current stimulation of prefrontal cortex. *Transl*
722 *Psychiatry* 3:e268.
- 723 Choi EY, Yeo BTT, Buckner RL (2012) The organization of the human striatum estimated by
724 intrinsic functional connectivity. *J Neurophysiol* 108:2242–2263.
- 725 Cole DM, Oei NYL, Soeter RP, Both S, van Gerven JMA, Rombouts SARB, Beckmann CF
726 (2013) Dopamine-dependent architecture of cortico-subcortical network connectivity.
727 *Cereb Cortex N Y N 1991* 23:1509–1516.
- 728 Damoiseaux JS, Rombouts SARB, Barkhof F, Scheltens P, Stam CJ, Smith SM, Beckmann
729 CF (2006) Consistent resting-state networks across healthy subjects. *Proc Natl Acad*
730 *Sci U S A* 103:13848–13853.
- 731 Desikan RS, Ségonne F, Fischl B, Quinn BT, Dickerson BC, Blacker D, Buckner RL, Dale
732 AM, Maguire RP, Hyman BT, Albert MS, Killiany RJ (2006) An automated labeling
733 system for subdividing the human cerebral cortex on MRI scans into gyral based
734 regions of interest. *NeuroImage* 31:968–980.
- 735 Düzel E, Bunzeck N, Guitart-Masip M, Wittmann B, Schott BH, Tobler PN (2009) Functional
736 imaging of the human dopaminergic midbrain. *Trends Neurosci* 32:321–328.
- 737 Flodin P, Gospic K, Petrovic P, Fransson P (2012) Effects of L-dopa and oxazepam on
738 resting-state functional magnetic resonance imaging connectivity: a randomized,
739 cross-sectional placebo study. *Brain Connect* 2:246–253.
- 740 Fonteneau C, Redoute J, Haesebaert F, Le Bars D, Costes N, Suaud-Chagny M-F, Brunelin
741 J (2018) Frontal Transcranial Direct Current Stimulation Induces Dopamine Release
742 in the Ventral Striatum in Human. *Cereb Cortex N Y N 1991*.

- 743 Fornai F, Chen K, Giorgi FS, Gesi M, Alessandri MG, Shih JC (1999) Striatal dopamine
744 metabolism in monoamine oxidase B-deficient mice: a brain dialysis study. *J*
745 *Neurochem* 73:2434–2440.
- 746 Foster HD, Hoffer A (2004) The two faces of L-DOPA: benefits and adverse side effects in
747 the treatment of Encephalitis lethargica, Parkinson's disease, multiple sclerosis and
748 amyotrophic lateral sclerosis. *Med Hypotheses* 62:177–181.
- 749 Frankle WG, Laruelle M, Haber SN (2006) Prefrontal Cortical Projections to the Midbrain in
750 Primates: Evidence for a Sparse Connection. *Neuropsychopharmacology* 31:1627–
751 1636.
- 752 Frazier JA, Chiu S, Breeze JL, Makris N, Lange N, Kennedy DN, Herbert MR, Bent EK,
753 Koneru VK, Dieterich ME, Hodge SM, Rauch SL, Grant PE, Cohen BM, Seidman LJ,
754 Caviness VS, Biederman J (2005) Structural brain magnetic resonance imaging of
755 limbic and thalamic volumes in pediatric bipolar disorder. *Am J Psychiatry* 162:1256–
756 1265.
- 757 Fryer SL et al. (2015) Relating Intrinsic Low-Frequency BOLD Cortical Oscillations to
758 Cognition in Schizophrenia. *Neuropsychopharmacology* 40:2705–2714.
- 759 Galvan A, Wichmann T (2008) Pathophysiology of Parkinsonism. *Clin Neurophysiol Off J Int*
760 *Fed Clin Neurophysiol* 119:1459–1474.
- 761 Goldstein JM, Seidman LJ, Makris N, Ahern T, O'Brien LM, Caviness VS, Kennedy DN,
762 Faraone SV, Tsuang MT (2007) Hypothalamic abnormalities in schizophrenia: sex
763 effects and genetic vulnerability. *Biol Psychiatry* 61:935–945.
- 764 Goto Y, Grace AA (2007) The dopamine system and the pathophysiology of schizophrenia: a
765 basic science perspective. *Int Rev Neurobiol* 78:41–68.

- 766 Haaker J, Gaburro S, Sah A, Gartmann N, Lonsdorf TB, Meier K, Singewald N, Pape H-C,
767 Morellini F, Kalisch R (2013) Single dose of L-dopa makes extinction memories
768 context-independent and prevents the return of fear. *Proc Natl Acad Sci* 110:E2428–
769 E2436.
- 770 Haber SN, Knutson B (2010) The Reward Circuit: Linking Primate Anatomy and Human
771 Imaging. *Neuropsychopharmacology* 35:4–26.
- 772 Hawrylycz MJ et al. (2012) An anatomically comprehensive atlas of the adult human brain
773 transcriptome. *Nature* 489:391–399.
- 774 Hedreen JC, DeLong MR (1991) Organization of striatopallidal, striatonigral, and nigrostriatal
775 projections in the macaque. *J Comp Neurol* 304:569–595.
- 776 Hilal-Dandan R, Brunton L (2014) Goodman and Gilman Manual of Pharmacology and
777 Therapeutics, 2. Auflage. New York: Mcgraw-Hill Education Ltd.
- 778 Hone-Blanchet A, Edden RA, Fecteau S (2016) Online Effects of Transcranial Direct Current
779 Stimulation in Real Time on Human Prefrontal and Striatal Metabolites. *Biol*
780 *Psychiatry* 80:432–438.
- 781 Kalivas PW, Volkow ND (2005) The neural basis of addiction: a pathology of motivation and
782 choice. *Am J Psychiatry* 162:1403–1413.
- 783 Kalu UG, Sexton CE, Loo CK, Ebmeier KP (2012) Transcranial direct current stimulation in
784 the treatment of major depression: a meta-analysis. *Psychol Med* 42:1791–1800.
- 785 Katzenschlager R, Lees AJ (2002) Treatment of Parkinson's disease: levodopa as the first
786 choice. *J Neurol* 249 Suppl 2:II19-24.
- 787 Leffa DT, de Souza A, Scarabelot VL, Medeiros LF, de Oliveira C, Grevet EH, Caumo W, de
788 Souza DO, Rohde LAP, Torres ILS (2016) Transcranial direct current stimulation

- 789 improves short-term memory in an animal model of attention-deficit/hyperactivity
790 disorder. *Eur Neuropsychopharmacol J Eur Coll Neuropsychopharmacol* 26:368–377.
- 791 Liu C-H, Liu C-Z, Zhang J, Yuan Z, Tang L-R, Tie C-L, Fan J, Liu Q-Q (2016) Reduced
792 spontaneous neuronal activity in the insular cortex and thalamus in healthy adults
793 with insomnia symptoms. *Brain Res* 1648:317–324.
- 794 Lu C, Wei Y, Hu R, Wang Y, Li K, Li X (2015) Transcranial Direct Current Stimulation
795 Ameliorates Behavioral Deficits and Reduces Oxidative Stress in 1-Methyl-4-Phenyl-
796 1,2,3,6-Tetrahydropyridine-Induced Mouse Model of Parkinson's Disease.
797 *Neuromodulation J Int Neuromodulation Soc* 18:442–446; discussion 447.
- 798 Maandag NJG, Coman D, Sanganahalli BG, Herman P, Smith AJ, Blumenfeld H, Shulman
799 RG, Hyder F (2007) Energetics of neuronal signaling and fMRI activity. *Proc Natl*
800 *Acad Sci* 104:20546–20551.
- 801 Makris N, Goldstein JM, Kennedy D, Hodge SM, Caviness VS, Faraone SV, Tsuang MT,
802 Seidman LJ (2006) Decreased volume of left and total anterior insular lobule in
803 schizophrenia. *Schizophr Res* 83:155–171.
- 804 Nitsche MA, Paulus W (2000) Excitability changes induced in the human motor cortex by
805 weak transcranial direct current stimulation. *J Physiol* 527 Pt 3:633–639.
- 806 Polanía R, Paulus W, Nitsche MA (2012) Modulating cortico-striatal and thalamo-cortical
807 functional connectivity with transcranial direct current stimulation. *Hum Brain Mapp*
808 33:2499–2508.
- 809 Power JD, Barnes KA, Snyder AZ, Schlaggar BL, Petersen SE (2012) Spurious but
810 systematic correlations in functional connectivity MRI networks arise from subject
811 motion. *Neuroimage* 59:2142–2154.

- 812 Rahman A, Reato D, Arlotti M, Gasca F, Datta A, Parra LC, Bikson M (2013) Cellular effects
813 of acute direct current stimulation: somatic and synaptic terminal effects. *J Physiol*
814 591:2563–2578.
- 815 Sánchez MG, Morissette M, Di Paolo T (2012) Effect of a chronic treatment with 17 β -
816 estradiol on striatal dopamine neurotransmission and the Akt/GSK3 signaling
817 pathway in the brain of ovariectomized monkeys. *Psychoneuroendocrinology* 37:280–
818 291.
- 819 Saturnino GB, Antunes A, Thielscher A (2015) On the importance of electrode parameters
820 for shaping electric field patterns generated by tDCS. *NeuroImage* 120:25–35.
- 821 Schwalm M, Schmid F, Wachsmuth L, Backhaus H, Kronfeld A, Aedo Jury F, Prouvot P-H,
822 Fois C, Albers F, van Alst T, Faber C, Stroh A (2017) Cortex-wide BOLD fMRI activity
823 reflects locally-recorded slow oscillation-associated calcium waves. *eLife* 6.
- 824 Takano Y, Yokawa T, Masuda A, Niimi J, Tanaka S, Hironaka N (2011) A rat model for
825 measuring the effectiveness of transcranial direct current stimulation using fMRI.
826 *Neurosci Lett* 491:40–43.
- 827 Thielscher A, Antunes A, Saturnino GB (2015) Field modeling for transcranial magnetic
828 stimulation: A useful tool to understand the physiological effects of TMS? In, pp 222–
829 225. IEEE. Available at: <http://ieeexplore.ieee.org/document/7318340/> [Accessed
830 May 27, 2018].
- 831 Valdés-Hernández PA, Sumiyoshi A, Nonaka H, Haga R, Aubert-Vásquez E, Ogawa T,
832 Iturria-Medina Y, Riera JJ, Kawashima R (2011) An in vivo MRI Template Set for
833 Morphometry, Tissue Segmentation, and fMRI Localization in Rats. *Front*
834 *Neuroinformatics* 5:26.

- 835 van Dam WO, Decker SL, Durbin JS, Vendemia JMC, Desai RH (2015) Resting state
836 signatures of domain and demand-specific working memory performance.
837 *NeuroImage* 118:174–182.
- 838 Volkow ND, Fowler JS, Gatley SJ, Logan J, Wang GJ, Ding YS, Dewey S (1996) PET
839 evaluation of the dopamine system of the human brain. *J Nucl Med Off Publ Soc Nucl*
840 *Med* 37:1242–1256.
- 841 Xu Y, Zhuo C, Qin W, Zhu J, Yu C (2015) Altered Spontaneous Brain Activity in
842 Schizophrenia: A Meta-Analysis and a Large-Sample Study. *BioMed Res Int*
843 2015:204628.
- 844 Yan C-G, Rincón-Cortés M, Raineke C, Sarro E, Colcombe S, Guilfoyle DN, Yang Z, Gerum
845 S, Biswal BB, Milham MP, Sullivan RM, Castellanos FX (2017) Aberrant development
846 of intrinsic brain activity in a rat model of caregiver maltreatment of offspring. *Transl*
847 *Psychiatry* 7:e1005.
- 848 Yarkoni T, Poldrack RA, Nichols TE, Van Essen DC, Wager TD (2011) Large-scale
849 automated synthesis of human functional neuroimaging data. *Nat Methods* 8:665–
850 670.
- 851 Zang Y-F, He Y, Zhu C-Z, Cao Q-J, Sui M-Q, Liang M, Tian L-X, Jiang T-Z, Wang Y-F (2007)
852 Altered baseline brain activity in children with ADHD revealed by resting-state
853 functional MRI. *Brain Dev* 29:83–91.
- 854 Zhou Y, Yu F, Duong TQ, Alzheimer's Disease Neuroimaging Initiative (2015) White matter
855 lesion load is associated with resting state functional MRI activity and amyloid PET
856 but not FDG in mild cognitive impairment and early Alzheimer's disease patients. *J*
857 *Magn Reson Imaging JMRI* 41:102–109.

858 Zou Q-H, Zhu C-Z, Yang Y, Zuo X-N, Long X-Y, Cao Q-J, Wang Y-F, Zang Y-F (2008) An
 859 improved approach to detection of amplitude of low-frequency fluctuation (ALFF) for
 860 resting-state fMRI: fractional ALFF. J Neurosci Methods 172:137–141.

861

862

863

864 **Table legends**

865

866 **Table 1: tDCS-induced effects in the mesostriatal system (voxel-wise analysis).** Peak
 867 voxels indicating tDCS-induced neural activity in the main as opposed to the inverse group in
 868 mesostriatal subregions. Coordinates are denoted by x,y,z in mm (MNI space). R: right, L:
 869 left, Caud: Caudate, NAcc: Nucleus Accumbens, Put: Putamen, SN/VTA: Substantia nigra /
 870 ventral tegmental area. p_{FWE} indicates small-volume FWE-corrected p-values for voxel-level
 871 inference.

872

873 **Table 2: L-DOPA-induced effects in the mesostriatal system (voxel-wise analysis).**
 874 Peak voxels indicating enhanced neural activity after L-DOPA as opposed to placebo
 875 administration in mesostriatal subregions after 45 and 90 minutes. Coordinates are denoted
 876 by x,y,z in mm (MNI space). For abbreviations, see Table 1. p_{FWE} indicates small-volume
 877 FWE-corrected p-values for voxel-level inference.

878

879 **Table 3: Comparison of dopamine receptor gene expression maps.** Pearson correlation
 880 coefficients (r) resulting from pairwise correlations of dopamine receptor gene expression
 881 maps (DRD1-DRD5).

882

883

884

885

886 **Figure legends**

887

888 **Figure 1: tDCS electric field simulation.** Anode placement over the frontopolar / ventro-
 889 medial prefrontal cortex (Fpz [red], left panel) and cathode placement over the right
 890 dorsolateral prefrontal cortex (F4 [blue], left panel) generated an electric field with maximal
 891 field strength in right lateral prefrontal areas (right panel).

892

893 **Figure 2: tDCS- and L-DOPA-induced effects in the mesostriatal system (ROI analysis).**

894 Using a human dopaminergic system mask (A), averaged fALFF increases were observed
 895 after tDCS in the main but not in the inverse group (B) and 90 min after L-DOPA
 896 administration (C). Boxplots show median, quartiles (boxes), and range (whiskers). Whiskers
 897 extend 1.5 times the interquartile range. Outliers are represented by dots. Asterisks indicate
 898 levels of statistical significance for interaction contrasts (tDCS: [tDCS_{main,post} - tDCS_{main,pre}] vs.
 899 [tDCS_{inv,post} - tDCS_{inv,pre}], L-DOPA: [LD_{90min} - LD_{0min}] - [Plc_{90min} - Plc_{0min}]) and Bonferroni-
 900 corrected post hoc *t*-tests (*, $p < 0.05$; **, $p < 0.01$; ***, $p < 0.001$).

901

902 **Figure 3: Spectral analysis.** Spectral analyses of the fMRI signal in the dopaminergic
 903 system revealed that both tDCS (A) and L-DOPA (B) amplified characteristic resting state
 904 frequencies (dashed lines: 0.01 to 0.08 Hz).

905

906 **Figure 4: L-DOPA-induced effects in the mesostriatal system of rats (ROI analysis).** In

907 rats, we found L-DOPA-induced fALFF increases after 45, 60 and 75 min when averaging
 908 across voxels in a dopaminergic system mask. Box plots show median, quartiles (boxes),
 909 and range (whiskers). Whiskers extend 1.5 times the interquartile range. Outliers are
 910 represented by dots. Asterisks indicate levels of statistical significance for uncorrected post
 911 hoc *t*-tests (*, $p < 0.05$; **, $p < 0.01$; ***, $p < 0.001$).

912

913 **Figure 5: tDCS- and L-DOPA-induced effects in the mesostriatal system (voxel-wise**
 914 **analysis).** tDCS-induced activation in the main as compared to the inverse group was
 915 restricted to areas of the dopaminergic system and most pronounced in the right putamen. L-
 916 DOPA as compared to placebo administration led to a significant activation of the SN/VTA
 917 after 45 min and of the left ventral striatum after 90 min. Green arrows indicate peak voxels.
 918 Small-volume FWE correction was performed for voxel-level inference. The display threshold
 919 was set to $p < 0.01$ (uncorrected).

920
 921 **Figure 6: Subcortical activation profiles.** tDCS and L-DOPA evoked similar subcortical
 922 activation profiles as revealed by a significant Pearson correlation of region-wise effect sizes
 923 (Cohen's d ; yellow: tDCS-induced effect; blue: L-DOPA-induced effect after 90 min; $r = 0.73$,
 924 $p = 0.002$). Labels were taken from the HO atlas. R: right, L: left, Hipp: Hippocampus, Amy:
 925 Amygdala, NAcc: Nucleus Accumbens, Pall: Pallidum, Thal: Thalamus, Caud: Caudate, Put:
 926 Putamen

927
 928 **Figure 7: gene-fALFF similarity profiles.** Each point indicates the z-transformed spatial
 929 correlation (similarity) of a particular gene expression map and the evoked activity pattern
 930 after tDCS (x-axis) and L-DOPA (y-axis, grey points: L-DOPA after 45 min; black points: L-
 931 DOPA after 90 min). Activity patterns induced by tDCS and L-DOPA after 90 min showed a
 932 pronounced similarity with gene expression patterns of the dopamine receptors D2 and D3
 933 (DRD2, DRD3; red circles) in comparison to other neuronal receptor genes. There was a
 934 significant linear relationship between gene-fALFF similarity values of tDCS and L-DOPA
 935 (grey line: L-DOPA after 45 min, $r = 0.82$; black line: L-DOPA after 90 min, $r = 0.88$), indicating
 936 analogous receptor-specific activation patterns for both interventions.

Tables**Table 1**

ROI	MNI [mm]	Cluster size	t-value	z-value	p_{FWE}
R Put	32 -8 0	286	5.25	4.52	0.002
L Caud	-14 16 4	58	4.18	3.77	0.026
L Put	-26 2 0	192	4.26	3.83	0.035
R Caud	12 10 10	15	3.98	3.61	0.043
SN/VTA	-10 -22 -12	7	3.59	3.31	0.045

966 **Table 2**

ROI	MNI [mm]	Cluster size	t-value	z-value	p _{FWE}
L-DOPA-induced activation after 45 min					
SN/VTA	-6 -14 -12	12	3.79	3.66	0.013
	-8 -24 -18	16	3.76	3.64	0.015
	6 -22 -20	10	3.67	3.55	0.019
L-DOPA-induced activation after 90 min					
L NAcc/Caud	-14 16 -8	11	3.91	3.77	0.004
R NAcc/Caud	14 18 -6	3	3.41	3.32	0.014
L Put	-28 -6 10	55	4.03	3.88	0.025

967

968

969

970

971

972

973

974

975

976

977

978

979

980

981

982

983

984

985

986

987 **Table 3**

	DRD1	DRD2	DRD3	DRD4	DRD5
DRD1	-	0.375	0.49	-0.07	0.39
DRD2	0.375	-	0.67	-0.06	0.1
DRD3	0.49	0.67	-	-0.16	0.04
DRD4	-0.07	-0.06	-0.16	-	0
DRD5	0.39	0.1	0.04	0	-

988

989

990

991

992

993

994

995

996

997

998

999

1000

1001

1002

1003

1004

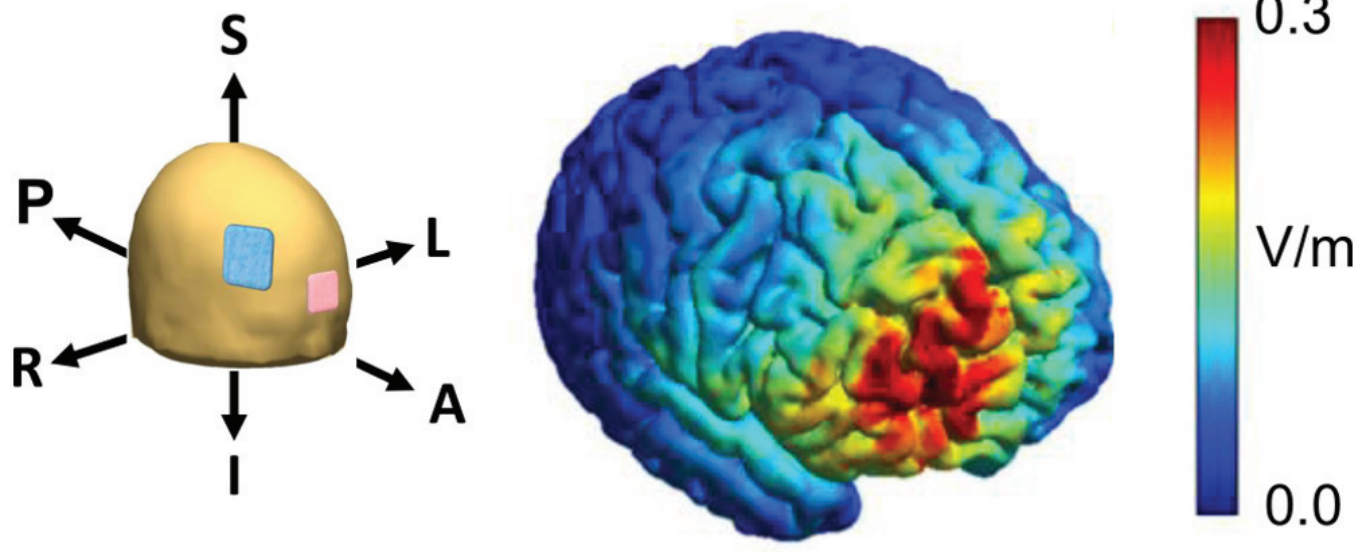
1005

1006

1007

1008

1009

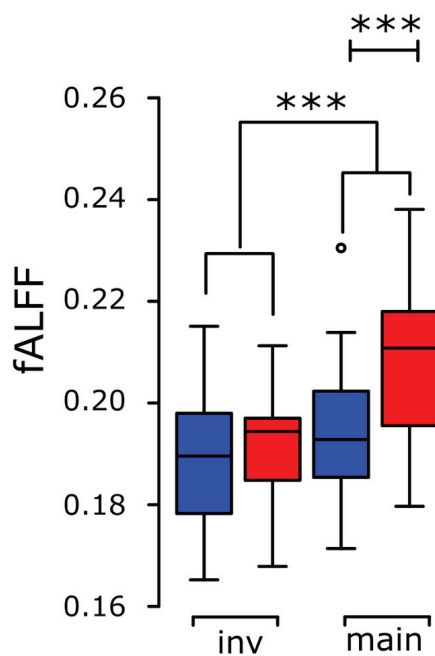


A



B

pre post



C

0 min 45 min 90 min

